Electronic Supplementary Material (ESI) for Physical Chemistry Chemical Physics.

Insights into the role of strontium in toluene catalytic combustion over $La_{1-x}Sr_xCoO_3$ perovskites catalysts

Mo Liu [a], Xiaoli Yang [a], Zimeng Tian [a], Huiming Wang [a], Liangtao Yin [a], Jianjun Chen [a], Qingqing Guan [a], Hao Yang [a]* , Qiulin Zhang [a]*.

[a] *Faculty of Environment Science and Engineering, Kunming University of Science and Technology, Kunming, 650500, China.*

Corresponding authors. Tel: +0086 13668788376

E-mail: qiulinzhang_kmust@163.com.

Corresponding authors. Tel: +0086 13350891007

E-mail: 948824189@qq.com

Supplementary table

Table S1. Comparison the catalytic performance of the $L_{0.82}S_{0.18}C$ catalyst with the reported catalysts mentioned in the literature.

Samples	Reaction conditions	Temperature (℃)	Conversion (%)	*Ea* (kJ /mol)	Reaction rate	References
$LaCoO_3$-149.52 kGy	1000 ppm toluene GHSV=20000 ml·(g cat)$^{-1}$·h-1).	280℃	97.08%	-	-	[1]
Ag/LCO	1000 ppm toluene, 30,000 $cm^3 \cdot g^{-1} \cdot h^{-1}$.	239℃	90%	-	4.19×10^{-3}(225℃)	[2]
LCO-20	1000 ppm toluene, 150000 ml· $g^{-1} \cdot h^{-1}$.	206℃	90%	46	15.3×10^{-8} mol·g^{-1}·s^{-1}	[3]
$La_{0.9}Ca_{0.1}CoO_3$-CA	1000ppm toluene, 60 000 mL ·g^{-1} ·h^{-1}.	202℃	90%	44.1	0.63 μmol $s^{-1}m^{-2}$	[4]
80Co-20La	500ppm toluene	242	90%	-	17.4 mmol $h^{-1}m^{-2}$) （220℃）	[5]
$La_{0.6}Sr_{0.4}Co_{0.9}Fe_{0.1}O3$	1000ppm toluene 20000 h^{-1}.	245 °C.	100%	-	-	[6]
$La_{0.75}Sr_{0.25}CoO_3$-d	500ppm toluene 30,000 L^{-1}·kg^{-1} ·h^{-1}	212	50%		11.6×10^{-9}mol s^{-1} m^{-2}	[7]
20 wt.% $LaCoO_3$/□-Al_2O_3.	900 ppm toluene 12000 L·Kg^{-1}·h^{-1}	300°C	100%	-	-	[8]
$L_{0.82}S_{0.18}C$	600ppm 20000 mL ·g^{-1} ·h^{-1}.	210	90%	69.1	3.2×10^{-7}mol·g^{-1}·s^{-1}	This article

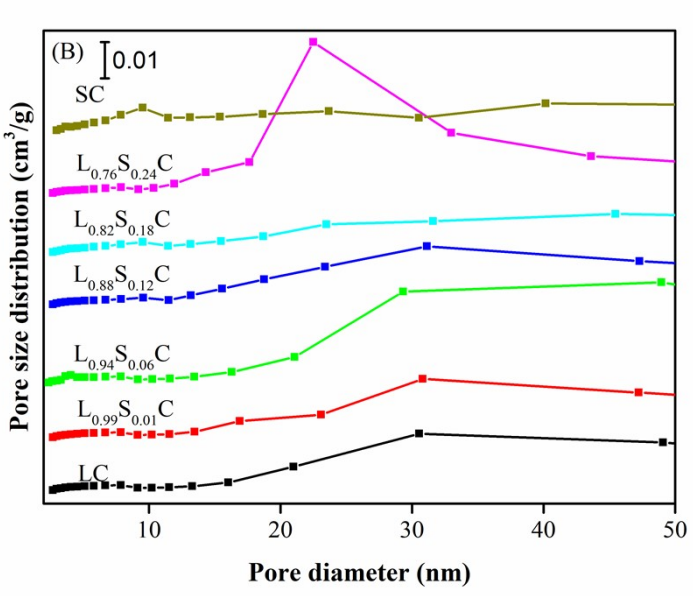

Fig. S1. The pore size distribution of the as-prepared samples.

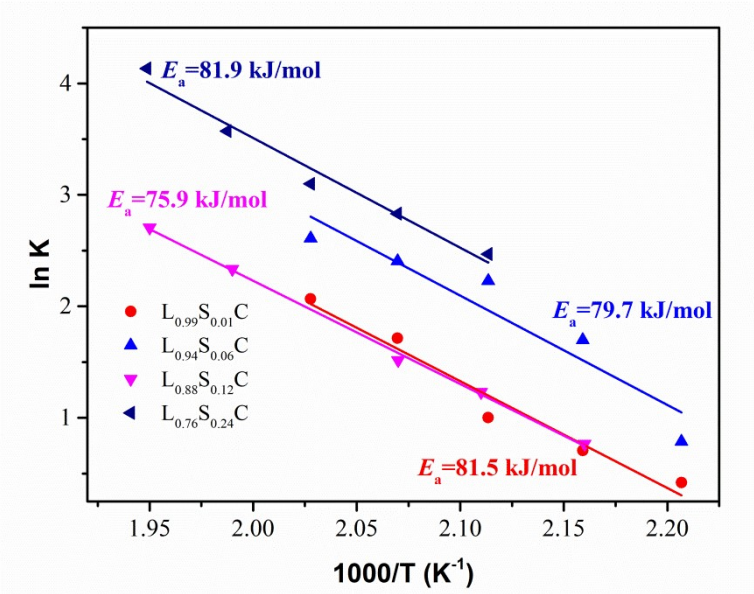

Fig. S2. Arrhenius plot of the logarithm of the toluene conversion rate constant and the reciprocal of the temperature.

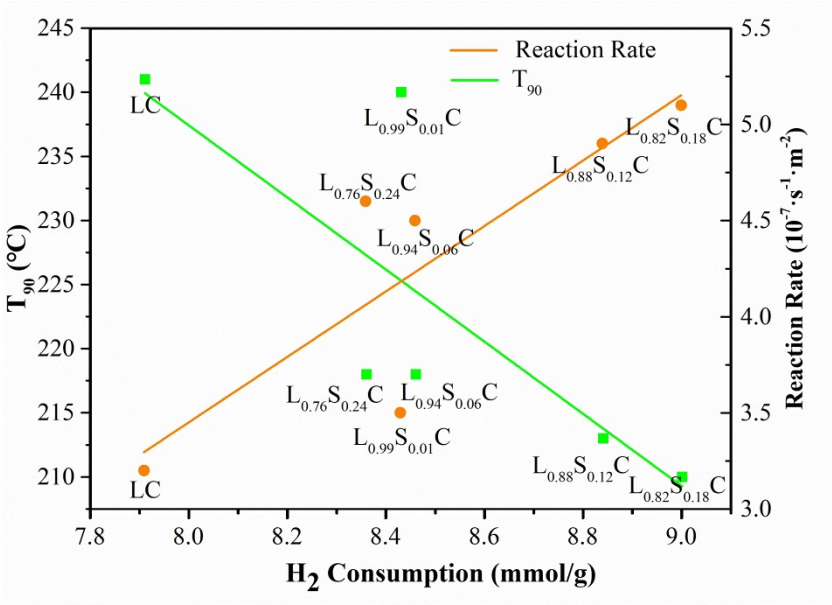

Fig. S3. Linear relationship between redox performance, T_{90} and conversion rate.

The in-situ DRIFTS were performed to investigate the catalytic mechanism of toluene oxidation over pervoskite catalysts. Firstly, we studied the adsorbed behavior of toluene on two catalysts under helium atmosphere, to eliminate the influence of oxygen. As shown in **Fig. S4**, peaks around 1619 and 1495 cm^{-1} [9] were assigned to the inplane skeletal vibration of aromatic ring. At the same time, the absorption intensity of benzaldehyde species (1593 and 1446 cm^{-1}) and benzoate species (1533 cm^{-1}) [9, 10], asymmetric vibration (1563 cm^{-1}) [11, 12] and symmetric vibration (1391 cm^{-1}) [13, 14] infrared peaks attributed to the benzoate species increased with the time increased, implying that toluene and intermediate product were easily adsorbed on both $L_{0.82}S_{0.18}C$ and LC samples. The peaks at 1619 cm^{-1} was attributed to the alcohol species (vibration of the C-O bond). All these peaks indicate that toluene adsorbed on LC and $L_{0.82}S_{0.18}C$ samples and converted into benzyl alcohol species by breaking the C-H bond.The peak around 3078 cm^{-1} was assign to the absorbed of benzene ring. It

is worth noting that the intensity of 3078 cm^{-1} [15] was increased with absorption time. During the purging process, an interesting phenomenon occurred. The infrared absorbed peaks attributed to the benzaldehyde species, benzyl alcohol species benzoate species and toluene are significantly reduced or disappeared. It shows that the intermediate product is easily removed on the surface of the catalyst. Obvious changes occurred during the helium purging process. Obviously, the absorption peak attributed to the benzene ring C-H quickly disappeared, and the peak of the intermediate product (benzaldehyde species, benzoate species) would also be significantly reduced. Comparing the two samples of LC and $L_{0.82}S_{0.18}C$, it can be clearly observed that the latter has more intermediate products. This confirms that XPS, $L_{0.82}S_{0.18}C$ among higher Co^{3+} content and more surface active oxygen species, which is more conducive to the catalytic oxidation of toluene.

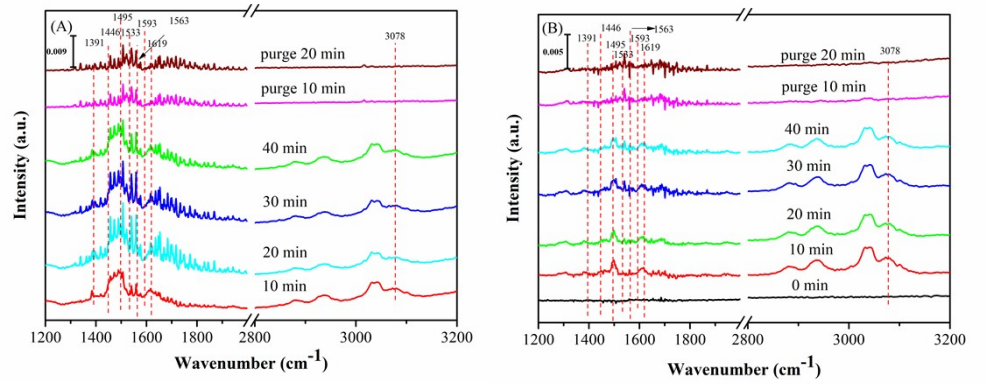

Fig. S4. Dynamic change of in-situ DRIFTS with the flow of 600 ppm toluene + He at 180 ℃. (a) $L_{0.82}S_{0.18}C$ and (b) LC catalyst.

We continue to study the effect of the two samples on the catalytic process of toluene as the reaction temperature changes, shown in **Fig. S5A** and **Fig. S5B**. For $L_{0.82}S_{0.18}C$ sample, the intensity of toluene and intermediate product gradually

increase with increase of temperature (50-150 °C). When the reaction temperature is 300 °C, it is basically difficult to observe the relevant infrared peaks attributable to the benzoate. As the reaction temperature increases, the peaks at 1619 cm^{-1} were attributed to the benzyl alcohol species was no obvious change for LC sample. However, the $L_{0.82}S_{0.18}C$ sample has an obvious decreasing trend at 250-400℃. Indicating toluene conversion to benzyl alcohol was the rate-controlling step of the reaction. As for LC sample, with the rise of temperature, peaks attributed to intermediate products increased with the reaction temperature. This means that the $L_{0.82}S_{0.18}C$ sample was easily to activate toluene molecule, which was beneficial to improve the catalytic performance.

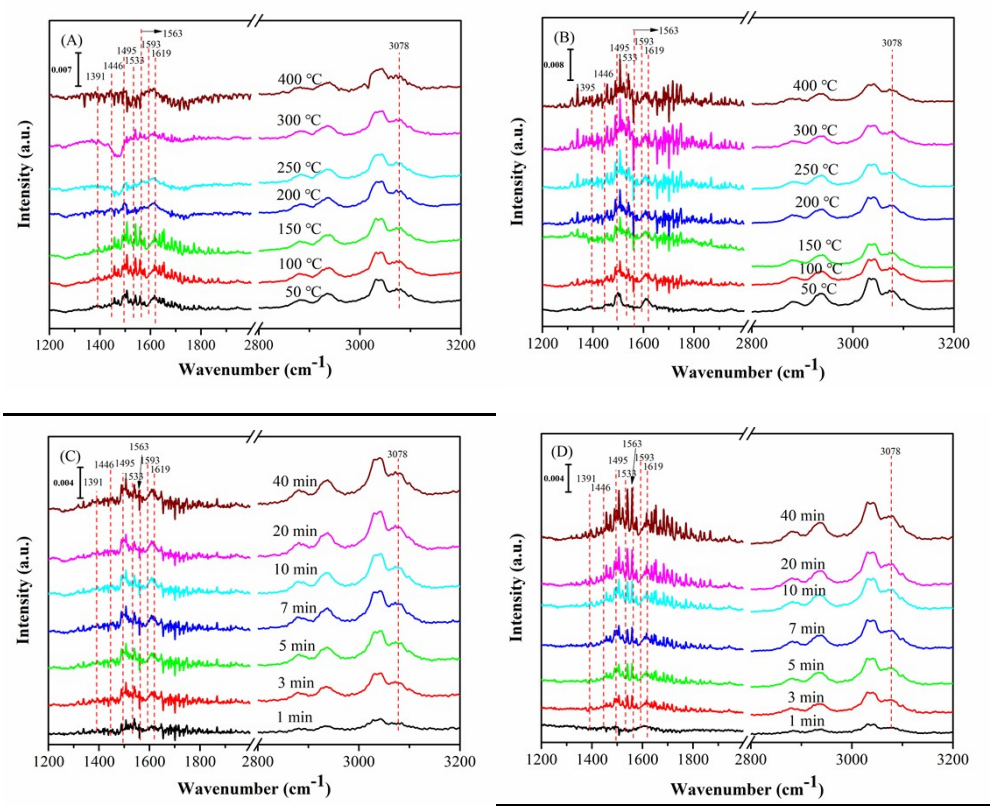

Fig. S5. Dynamic change of in-situ DRIFTS over temperature in the flow of 600 ppm toluene + 21

vol.% O_2 + He, (A) different temperature reaction of $L_{0.82}S_{0.18}C$ sample. (B) different temperature reaction of LC catalyst. (C) $L_{0.82}S_{0.18}C$ at 180 ℃. (D) LC at 220 ℃.

We could reasonable to infer that the 220 ℃ and 180 ℃ was the most sense temperature of LC and $L_{0.82}S_{0.18}C$ sample，according to the results of **Fig. S5A** and **Fig. S5B**. Therefore, we conduct the in-situ DRIFTS dynamic reactions of LC and $L_{0.82}S_{0.18}C$ catalysts at 220 °C and 180 °C with the reaction time. As shown in **Fig. S5C**, for the $L_{0.82}S_{0.18}C$ sample, with the increase of reaction time, the infrared peaks belong to intermediate species (benzaldehyde species, benzyl alcohol species benzoate species) were gradually increased, and there was no obvious change after seven minutes of reaction. It shows that the intermediate product did not on the surface of the $L_{0.82}S_{0.18}C$ sample. For the LC sample, intermediate products accumulated on the surface of the catalyst, and it gradually increased with reaction time (seen in **Fig. S5D**).

Therefore, for the reaction mechanism, it can be reasonably inferred that toluene is first adsorbed on the surface of the catalyst and oxidized by surface oxygen species to form benzyl alcohol species, and further oxidized to form benzaldehyde and benzoic acid species. The benzoic acid species will be oxidized in an oxygen atmosphere to form formate species, and further oxidized to form carbon dioxide and water. Toluene conversion to benzyl alcohol was the rate-controlling step of the reaction.

References

1. X. Fei, W. Jia, Z. Hou, H. Dai, Q. Shan, D. Hei and Y. Ling, *Radiat. Phys. Chem.*, 2019, **158**, 143-147.

2. H. Chen, G. Wei, X. Liang, P. Liu, H. He, Y. Xi and J. Zhu, *Appl. Surf. Sci.*, 2019, **489**, 905-912.

3. H. Chen, W. Cui, D. Li, Q. Tian, J. He, Q. Liu, X. Chen, M. Cui, X. Qiao, Z. Zhang, J. Tang and Z. Fei, *Ind. Engin. Chem. Res.*, 2020, **59**, 10804-10812.

4. H. Chen, G. Wei, X. Liang, P. Liu, Y. Xi and J. Zhu, *Catal. Sci. Techn.*, 2020, **10**, 5829-5839.

5. Z. Huang, M. Zhao, J. Luo, X. Zhang, W. Liu, Y. Wei, J. Zhao and Z. Song, *Sep. Purif. Technol.*, 2020, **251**, 117369.

6. J. Deng, H. Dai, H. Jiang, L. Zhang, G. Wang, H. He, C. Au, *Environ. Sci. Techn.,* 2010, 44, 2618-2623.

7. R. Pereñíguez, J. L. Hueso, F. Gaillard, J. P. Holgado and A. Caballero, *Catal. Lett.*, 2012, **142**, 408-416.

8. K. Matsuo, N. Nunotani and N. Imanaka, *Funct. Mater, Lett.*, 2020, **13**, 1-4.

9. X. Lai, X. Zhou, H. Zhang, X. Jiang, T. Lin and Y. Chen, *Appl. Surf. Sci.*, 2020, **526**, 146714.

10. C. Zhao, Q. Hao, Q. Zhang, N. Yan, J. Liu, B. Dou and F. Bin, *Appl. Catal. A Gen.*, 2019, **569**, 66-74.

11. X. Chen, X. Chen, E. Yu, S. Cai, H. Jia, J. Chen and P. Liang, *Chem. Eng. J.*, 2018, **344**, 469-479.

12. A. Lu, H. Sun, N. Zhang, L. Che, S. Shan, J. Luo, J. Zheng, L. Yang, D.-L. Peng, C.-J. Zhong and B. Chen, *ACS Catal.*, 2019, **9**, 7431-7442.

13. Y. Wang, G. Wang, W. Deng, J. Han, L. Qin, B. Zhao, L. Guo and F. Xing, *Chem. Eng. J.*, 2020, **395**.

14. X. Yang, X. Yu, M. Jing, W. Song, J. Liu and M. Ge, *ACS Appl. Mater. Interfaces*, 2019, **11**, 730-739.

15. J. Chen, X. Chen, W. Xu, Z. Xu, J. Chen, H. Jia and J. Chen, *Chem. Eng. J.*, 2017, **330**, 281-293.